Journal of Molecular Graphics and Modelling 27 (2009) 829–835

Contents lists available at ScienceDirect

Journal of Molecular Graphics and Modelling

journal homepage: www.elsevier.com/locate/JMGM

Bridging the gap between molecular descriptors and mechanism: Cases studies by molecular dynamics simulations

Liang Xu [a,b], Xicheng Wang [b,*], Weijie Zhao [c]

[a] Department of Engineering Mechanics, State Key Laboratory of Structural Analyses for Industrial Equipment, Dalian University of Technology, Dalian 116023, China
[b] Department of Chemistry, Dalian University of Technology, Dalian 116023, China
[c] School of Chemical Engineering, State Key Laboratory of Fine Chemicals, Dalian University of Technology, Dalian 116012, China

ARTICLE INFO

Article history:
Received 1 September 2008
Received in revised form 17 December 2008
Accepted 30 December 2008
Available online 12 January 2009

Keywords:
Support vector machine
Molecular dynamics
Mechanism of toxic action
Uncoupling activity
Polar narcotics

ABSTRACT

In recent years, both classification models and quantitative structure–activity relationships (QSARs) have been developed to discriminate the acute toxicity of polar narcotics and uncouplers. One of fundamental issues is how to select and interpret the molecular descriptors used in both methods. In this work, we first employed support vector machine on a dataset containing 155 polar narcotics and 19 uncouplers to filter the predictive hydrophobic and hydrogen bonding descriptors. Molecular dynamics simulations were then conducted to investigate the behavior of salicylate and pentachlorophenol molecules in the context of a palmitoyl-oleoyl-phosphatidylcholine lipid bilayer. The results demonstrated that their equilibrium properties in the lipid bilayer were closely associated with hydrophobic and hydrogen bonding descriptors. The preferable occupations of these molecules in the lipid bilayer were discussed in terms of their modes of toxic action. The observations from molecular dynamics simulations facilitated to elucidate the mechanism of polar narcotics and uncouplers.

1. Introduction

Understanding the mechanism of toxic action (MOA) of phenols is an important but difficult problem [1]. Phenols and their derivatives are ubiquitous environmental contaminants and toxic to many organisms by interfering energy transduction in cells [2–4]. Direct experimental measurement of the potential toxicity is both expensive and time-consuming [5]. With different substitutions, phenols may exert various biological activities. Besides, one kind of toxicity may be caused by the superposition of effects from different mechanisms. Despite the complex bioreactivity patterns, four important mechanisms of toxic action of phenols, i.e., polar narcotics, weak acid respiratory uncouplers, proelectrophiles and soft electrophiles, have been established and studied extensively. Structural characterization for each MOA has been proposed in previous publications [6–12]. In brief, the distinct features of polar narcotics are their hydrophobic and hydrogen bond donor capacities that allow them to accumulate in lipid tissues and cause unspecific membrane irritation. Uncouplers, with moderate hydrophobicity and acidity, have ability to inhibit ATP synthesis in energy producing membranes [6,11,12]. There is not a clear understanding of proelectrophiles and soft electrophiles to date, making it problematic to classify or quantitatively predict the two MOAs [11,12].

Both classification (qualitative) and quantitative structure–activity relationship (QSAR) (quantitative) approaches have currently been applied to predict the toxicity of chemicals [13]. For instance, the dataset with 221 phenols presented in the study of Aptula et al. [7] has been validated to be suitable for developing models. Classification models based on statistical learning methods have been applied to this dataset by using various molecular descriptors [9,11,12]. Such methods are straightforward and need no experimental data while phenols with more than one MOA cannot be predicted reliably. QSARs also rely on many calculated molecular descriptors whose predictive ability may vary with different calculation methods, variable selection algorithms and optimization of the training procedure [13,14]. In addition, some descriptors are difficult to interpret in terms of the MOA for both methods [15–17].

One hydrophobic descriptor ($\log K_{ow}$, see Section 2 for further details) and six hydrogen bonding descriptors (E_{HOMO}, E_{LUMO}, D^{E}_{C-max}, D^{N}_{C-av}, N_{Hdon}, and N_{Hacc}) have been used to classify 220 phenols into four MOAs by Schüürmann et al. [11]. Other studies have also demonstrated that both hydrophobic and hydrogen bonding descriptors are relevant [7,9,12,18]. Additionally the development of QSARs for the aquatic toxicity of polar and

* Corresponding author. Tel.: +86 411 84706223; fax: +86 411 84708393.
E-mail address: guixum@dlut.edu.cn (X. Wang).

1093-3263/$ – see front matter.
doi:10.1016/j.jmgm.2008.12.007

nonpolar narcotics has indicated that the toxicity of narcotics is associated with the hydrophobic [19–21] and hydrogen bonding capability [19,20,22].

However, it seems still difficult to predict the toxicity from molecular structures by current methods [23]. Combined with experimental data, the primary target site for the acute toxicity of substituted phenols in aquatic organisms has been proposed to be the membrane [3,4,6]. A clear insight into the interaction at the target is thus desirable in developing models and guiding to select relevant molecular descriptors. Furthermore, the knowledge of the interaction between an xenobiotic compound and biological membrane is also crucial for subcelluar pharmacokinetics and rational drug design [24]. Yet, such atomic detailed information cannot be accessible to QSARs or experiments. Molecular dynamics (MD) simulation, which serves as an excellent complement to experimental researches, can help to understand the dynamic behavior of small molecules in lipid bilayer at atomic level and thus can provide important implications for those molecular descriptors.

In this paper, MD simulations were conducted to study the equilibrium properties of two representative phenol derivatives, i.e., pentachlorophenol (PCP) and salicylate (SAL), in a palmitoyl-oleoyl-phosphatidylcholine (POPC) lipid bilayer. PCP is a typical uncoupler that is toxic to cell membrane by inhibiting the electron transport or destroying the electrochemical proton gradient built up across membranes [3,4]. Evidences also show that such uncoupling activity depends strongly on the speciation of phenols inside the membrane [3,4]. The distribution of neutral PCPs in a POPC bilayer has been studied by MD simulation previously [25]. Considering the membrane-water partition coefficient and acidity constant ($pK_a = 4.75$) of PCPs [3,4], ionized PCPs were used in the present MD simulations. Although the target of polar narcotics (e.g. SALs), as stated above, is not so clear as uncouplers, SALs have been suggested to interact with phospholipid bilayers and some membrane-bound proteins [26]. MD simulations have also indicated that the perturbation of SALs on a model membrane dipalmitoylphosphatidylcholine (DPPC) could be useful to understand the hearing-related side effects in the context of the cochlear outer hair cell membrane mechanical and electrical properties [26].

We first give here the results of binary classification of polar narcotics and uncouplers using support vector machine (SVM), which evaluate the discriminative capability of hydrophobic and hydrogen bonding descriptors. MD simulations are then performed to investigate the interaction of PCP and SAL molecules in POPC bilayers, respectively. In particular, the properties of hydrogen bonding are characterized. These results allow us to discuss the different toxic effects of polar narcotics and uncouplers.

2. Methodology

2.1. Binary classification

The dataset used in this study is the same as used by Spycher et al. [12] but contains only two MOAs, i.e., 155 polar narcotics and 19 uncouplers. The molecular descriptors are the octanol/water partition coefficient, $\log K_{ow}$; the energy of the highest occupied molecular orbital, E_{HOMO}; the energy of the lowest unoccupied molecular orbital, E_{LUMO}; the highest electrophilic delocalizability of a carbon atom, D^{E}_{C-max}; the average carbon atom nucleophilic delocalizability, D^{N}_{C-av}; the number of hydrogen bond donors, N_{Hdon} and the number of hydrogen bond acceptors, N_{Hacc} [11]. SVM was used as the binary classification method due to its remarkable advantages over many other methods [27]. Extensive applications of SVM in classification and QSAR analysis have made it one of popular machine-learning methods in recent years. Therefore, a description of the algorithm seems unnecessary and can be found elsewhere [28]. The freely available software LIBSVM [29] with radial basis function (RBF) as the kernel was employed. The optimal penalty parameter C and the RBF parameter γ were determined automatically by using the grid.py script [29]. Classification results were evaluated with 5-fold cross validation (CV) method and the whole procedure was repeated 5–100 times, with the dataset reshuffled each time in order to reduce the variation caused by random splitting.

2.2. Molecular dynamics simulations

The structures of ionic SAL, PCP, and POPC are shown in Fig. 1. The structures of SAL and PCP were first optimized using Gaussian 03 program at the HF/6-31G* level and the electrostatic potential was calculated at the same level using the MK scheme [30]. The restrained electrostatic potential (RESP) method was then used to fit the electrostatic potential [31]. The atomic partial charges are listed in Supplementary Material, Table S1. We notice that the partial charges of SAL are comparable to those calculated by quantum mechanical/molecular mechanical procedures [26]. The united atom topology files for SAL and PCP were generated by using the PRODRG server [32]. The pure POPC lipid bilayer structure available at http://moose.bio.ucalgary.ca/files/popc128b.pdb was taken as starting configuration, which contains 128 POPC lipids (i.e., 64 lipids in each leaflet) and 2460 waters, corresponding to 19 water molecules per lipid, that is, a fully hydrated state of the lipid [33]. The force field parameters of lipid were taken from Berger et al. [34]. The single point charge (SPC) model for water was used in all the simulations below [35]. These parameters have been shown to accurately reproduce the experimental area per lipid and the deuterium order parameters [25,35,36].

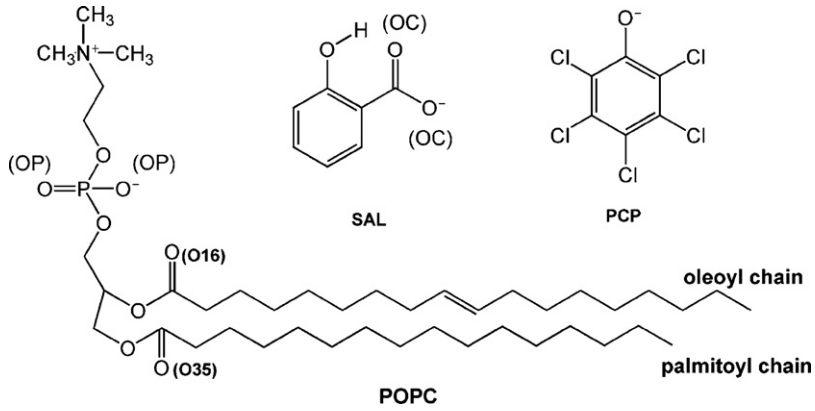

Fig. 1. The chemical structure of POPC, SAL and PCP, as well as the oxygen atom notation used throughout this paper.

Six ionized SAL or PCP (SAL/PCP) molecules were inserted manually into the membrane in the lipid–water interface region, with three molecules in each leaflet. In each simulation, six water molecules were replaced with six Na^+ ions to neutralize the overall system. All bond lengths were constrained using the LINCS algorithm, allowing a time steps of 2 fs [37]. Each system was first minimized for 2000 steps to avoid unfavorable van der Waals contacts, and then heated to 310 K through 20 ps in the NPT ensemble with anisotropic pressure coupling (τ_P = 1.0 ps) to 1 bar in each direction and temperature coupling (τ_t = 0.1 ps) of lipid, water, Na^+ and SAL/PCP separately. Both temperature and pressure were controlled by Berendsen coupling protocols [38]. The Lennard–Jones cutoff was set at 0.9 nm and the full electrostatics interactions were computed with the particle mesh Ewald (PME) method [39,40]. MD simulations and analyses were carried out by using the GROMACS 3.3.1 software package [41]. For each MD run, 50 ns production trajectory was produced in the same NPT ensemble. For comparison, another 50 ns MD simulation of the neat POPC bilayer was performed under the same conditions as well.

3. Results and discussion

3.1. Results of SVM classification

Binary classification results involved one to seven descriptors are shown in Fig. 2 and Table 1, as well as the results of eight models (A–H in Table 1) for each compound are summarized in Supplementary Material, Table S2.

The high stability of the results indicates that the effect due to random splitting of the dataset is negligible. The largest standard deviation in the present test is only 0.14% as listed in Table 1(B). The predictive capability of these seven descriptors is also confirmed by the average accuracy of 98.28% (C).

Since the 155 polar narcotics are 89.08% of the 174 phenols, it can be seen that $\log K_{ow}$ used alone has no discriminative ability because predicting any phenol as a polar narcotic can lead to a correction of 89.08% on the average (H). Interestingly, it is found that when $\log K_{ow}$ used together with other two descriptors (E and G) the classification rates are slightly lower than those without $\log K_{ow}$ (D and F) but higher than the case where only $\log K_{ow}$ was used (H). Such results are in good agreement with previous QSAR or classification studies on the toxicity of narcotics, which assumed the toxicity of narcotics was mainly determined by the hydrophobicity of the chemicals [13,19,21,42]. However, only descriptor $\log K_{ow}$ was not sufficient to describe the toxicity, and the higher

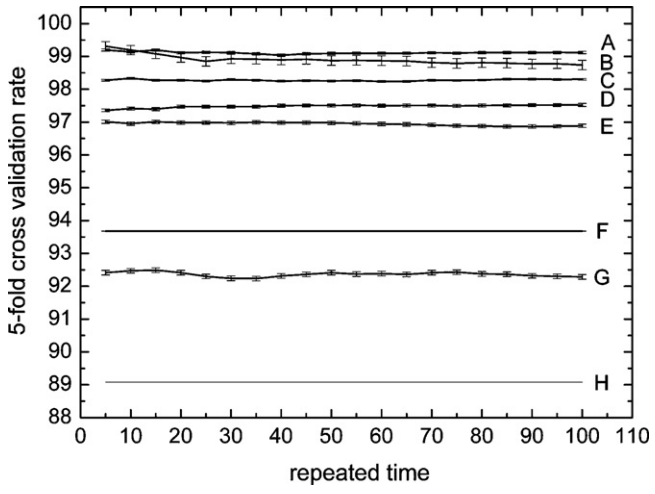

Fig. 2. SVM classification results. Vertical bars indicate the standard errors.

Table 1
SVM classification rates with different descriptors.

Curve	Molecular descriptors	CV rate (%)
A	E_{HOMO}, E_{LUMO}, N_{Hdon}, N_{Hacc}	99.11 ± 0.04
B	$\log K_{ow}$, E_{HOMO}, E_{LUMO}, N_{Hdon}, N_{Hacc}	98.90 ± 0.14
C	$\log K_{ow}$, E_{HOMO}, E_{LUMO}, D^E_{C-max}, D^N_{C-av}, N_{Hdon}, N_{Hacc}	98.28 ± 0.03
D	E_{HOMO}, E_{LUMO}	97.48 ± 0.04
E	$\log K_{ow}$, E_{HOMO}, E_{LUMO}	96.94 ± 0.05
F	N_{Hdon}, N_{Hacc}	93.68 ± 0.00
G	$\log K_{ow}$, N_{Hdon}, N_{Hacc}	92.36 ± 0.07
H	$\log K_{ow}$	89.08 ± 0.00

toxicity of polar narcotics than nonpolar ones was attributed to E_{LUMO} which was another important parameter in developing QSARs or classifying toxic compounds [13,19,42]. Furthermore, the importance of H-bond donor capacity referred to as N_{Hdon} was highlighted in QSARs for polar narcotics [21]. In the present study, we take the POPC lipid bilayer as the target for polar narcotics and uncouplers and employ the united-atom representation for the POPC bilayer, thus the hydrogen acceptor contribution of phenols (N_{Hacc}) was not taken into account alone. On the other hand, as pointed out by other studies, the E_{HOMO} represented the convalent contribution to hydrogen bonding for the acceptor [19,20]. The POPC bilayer was considered as the H-bond acceptor here, therefore E_{HOMO} was not tested as a single descriptor either.

Minor difference is found when including D^E_{C-max} and D^N_{C-av} in classification tests (B and C), indicating these two descriptors could be of less importance in differentiating polar narcotics from uncouplers. Moreover, the introduction of $\log K_{ow}$ into other four descriptors related to hydrogen bonding yields almost the same correct prediction (A and B). These findings are consistent with the results obtained by Schüürmann et al. [11] In their studies, E_{HOMO} and D^E_{C-max} were suitable to discriminate between polar narcotics and proelectrophiles, and $\log K_{ow}$ and D^N_{C-av} were reasonable descriptors to separate uncouplers from soft electrophiles. Phenols assigned as proelectrophiles and electrophiles were not investigated here because their possible targets are much ambiguous, as mentioned in Section 1. Another interesting result is that the performance of four hydrogen bonding descriptors is apparently superior to $\log K_{ow}$, suggesting different pattern of hydrogen bonding between polar narcotics and uncouplers (A and H).

The results of SVM classification demonstrate that the predictive ability of hydrophobic and hydrogen bonding descriptors is significant. In the following MD simulations, we choose SAL and PCP as examples to gain more insight into the related mechanisms underlying these descriptors.

3.2. Results of MD simulations

The number of contacts between SAL/PCP molecules and the lipid is used as a measure to monitor if the two systems have reached equilibrium. As suggested, a contact occurs when the distance between any atom of the SAL/PCP and any atom of the POPC bilayer is less than 0.6 nm [43]. Fig. 3 indicates that after 30 ns and 35 ns the SALs and PCPs have almost reached their equilibrium positions in the POPC bilayer for both simulations. The trajectory of the center of the mass of every SAL in the SAL–POPC system showed that one SAL diffused from one leaflet to the other leaflet of the bilayer and remained there for the last 20 ns (data not shown). Similar migration was observed in the PCP–POPC system, with one PCP diffusing between two leaflets of the bilayer after 20 ns. Interestingly, no aggregation formed by SALs was observed. Therefore, the last 20 ns SAL–POPC and 15 ns PCP–POPC trajectories were used for further analyses of the two simulations.

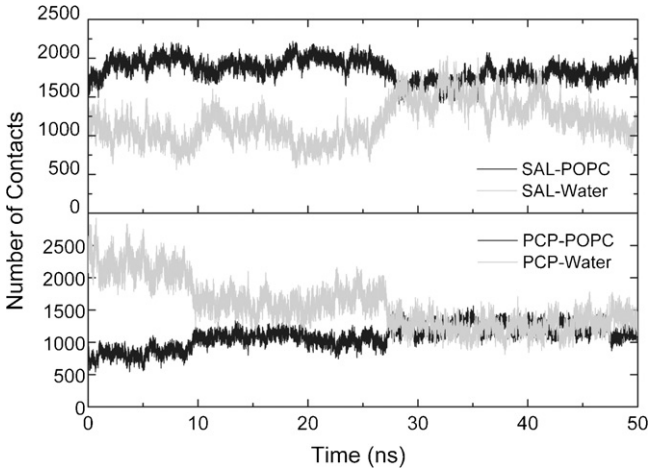

Fig. 3. Number of contacts between SAL/PCP molecules and the POPC bilayer. Number of contacts between SAL/PCP molecules and water is also shown for discussion.

Table 2
Area per lipid (nm^2) for POPC with and without small molecules, as well as experimental (Exp.) and MD simulation values.

PCP–POPC	SAL–POPC	POPC	POPC (Exp./MD)
	0.678 ± 0.011	0.683 ± 0.011 (20 ns)	0.683 ± 0.015 (303 K, Exp.) [44]
0.678 ± 0.010		0.681 ± 0.011 (15 ns)	0.684 ± 0.005 (310 K, MD) [45]

Equilibrium properties described by area per lipid, electron density of different components, were calculated and compared with the results obtained from the pure POPC simulation and previous studies. The average area per lipid for the SAL–POPC, PCP–POPC and pure POPC are summarized in Table 2. The area per lipid of pure POPC is fully consistent with the experimental and previous simulation value [44,45]. The results suggest that the presence of SAL/PCP molecules yields insignificant reduction in the area per lipid because of the lower concentration of SAL/PCP molecules compared with previous studies [25,26].

The electron density profiles of SAL–POPC and PCP–POPC systems shown in Fig. 4 are quite similar for the distribution of

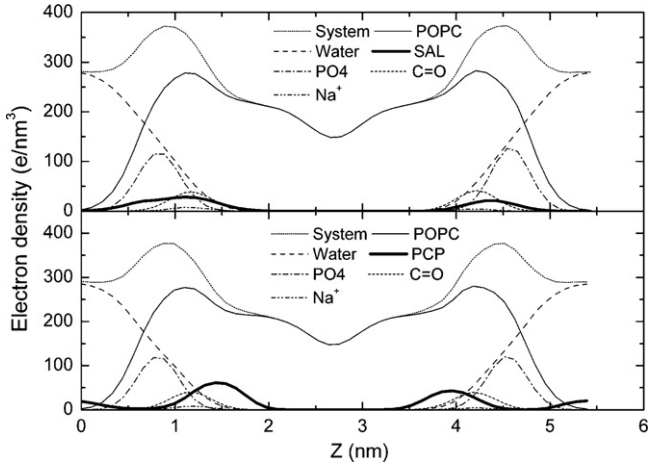

Fig. 4. Electron density profiles along the bilayer normal (Z) calculated for different components of the two systems. The density curves of PCPs and Na^+ have been multiplied by a factor of 5 for clarity. The density profiles are averaged over the last 20 ns and 15 ns of the trajectories from SAL–POPC and PCP–POPC simulations, respectively.

POPC, water and phosphate groups, indicating the perturbation caused by SAL/PCP molecules is not obvious. The electron density of SAL/PCP molecules is not symmetrical with respect to the two leaflets of the POPC bilayer due to the uneven distribution of SAL/PCP molecules in each leaflet. Most notably, for the SAL–POPC system, the density of SALs has overlap with the carbonyl and phosphate groups, which indicates that the preferred position of SALs in the POPC bilayer lies in the lipid headgroup. For the PCP–POPC system, PCPs reside in the region between carbonyl groups and water phase (lipid–water interface). It should be noted that the distribution of neutral and ionized PCPs in the POPC bilayer is different because neutral PCPs have been observed to preferably occupy the region between carbonyl groups and the double bonds in the alkyl chains of the POPC bilayer [25]. Fig. 4 also indicates that Na^+ ions could coordinate with SALs and PCPs, which partly explains the decrease in the number of contacts between SAL and water during the last 10 ns as shown in Fig. 3.

Taking present and previous MD simulations together, we find that neutral PCPs penetrate into the lipid bilayer, SALs reside in the region of lipid headgroup and ionized PCPs tend to occupy the region of lipid–water interface. Available experimental data for octanol–water partition coefficient ($\log K_{ow}$) of neutral PCPs is 5.24 and liposome-water partition coefficients ($\log K_{lipw}$) of the nondissociated and the dissociated PCPs are 5.09 and 4.49, respectively [46]. As expected, the values of calculated $\log K_{ow}$ and experimental $\log K_{lipw}$ for PCPs are in accordance with the results of MD simulations. The nondissociated PCPs, with larger $\log K_{lipw}$ (or $\log K_{ow}$) values, partition more deeply into the lipid phase.

Evidence from experiments implies that the speciation inside the membrane is the pivotal factor for the protonophoric activity of uncouplers. The proposed mechanism of protonophoric action involves the so-called "shuttle cycle" process [6,46,47]. The anionic form of uncouplers driven by membrane potential diffuses through the membrane from negatively charged side (n-side) to the positively charged side (p-side), therefore, decreasing the potential. On the p-side, the anionic uncoupler binds a proton (H^+) at the membrane–water interface and becomes the neutral form. Then, the protonated neutral uncouplers passively diffuse back to the n-side and release a proton. By this cycle, a proton is transferred across the membrane. To exert these effects, the stability of uncouplers in the membrane is considered to be important. Thus, the distributions of neutral and anionic form of PCPs in the POPC bilayer at equilibrium from MD simulations provide an important validation for the above mechanism.

The calculated values of $\log K_{ow}$ for neutral and anionic SALs are 2.19 [7,11] and −2.88 [8], respectively. As well, it seems possible to conclude that neutral SALs penetrate more deeply into the lipid bilayer. However, there is little experimental data available to verify the existence of neutral SALs in membrane, MD simulation of neutral SALs in POPC bilayer was not conducted. The present MD simulations demonstrate that dissociated SALs diffuse deeper than dissociated PCPs in the POPC bilayer, while the calculated $\log K_{ow}$ for anionic SALs (−2.88) [8] is smaller than anionic PCPs (2.11) [8]. This discrepancy suggests that $\log K_{ow}$ and $\log K_{lipw}$ may not always be equivalent.

In order to examine the interaction of SAL/PCP molecules within the POPC bilayer, radial distribution functions (RDFs) for the potential hydrogen bonding partners and charge pairing around SAL and PCP molecules were calculated and shown in Fig. 5. In this work, we adopt the commonly used geometric criteria to define a hydrogen bond (H-bond), i.e., the acceptor-hydrogen distance is less than 0.24 nm and the donor-hydrogen-acceptor angle is less than 90. Inspection of the distance where the first peak occurs in the RDFs indicates the formation of H-bond.

In Fig. 5, there is H-bond established between the hydrogen atom of hydroxyl group and oxygen atoms of carboxylic group in

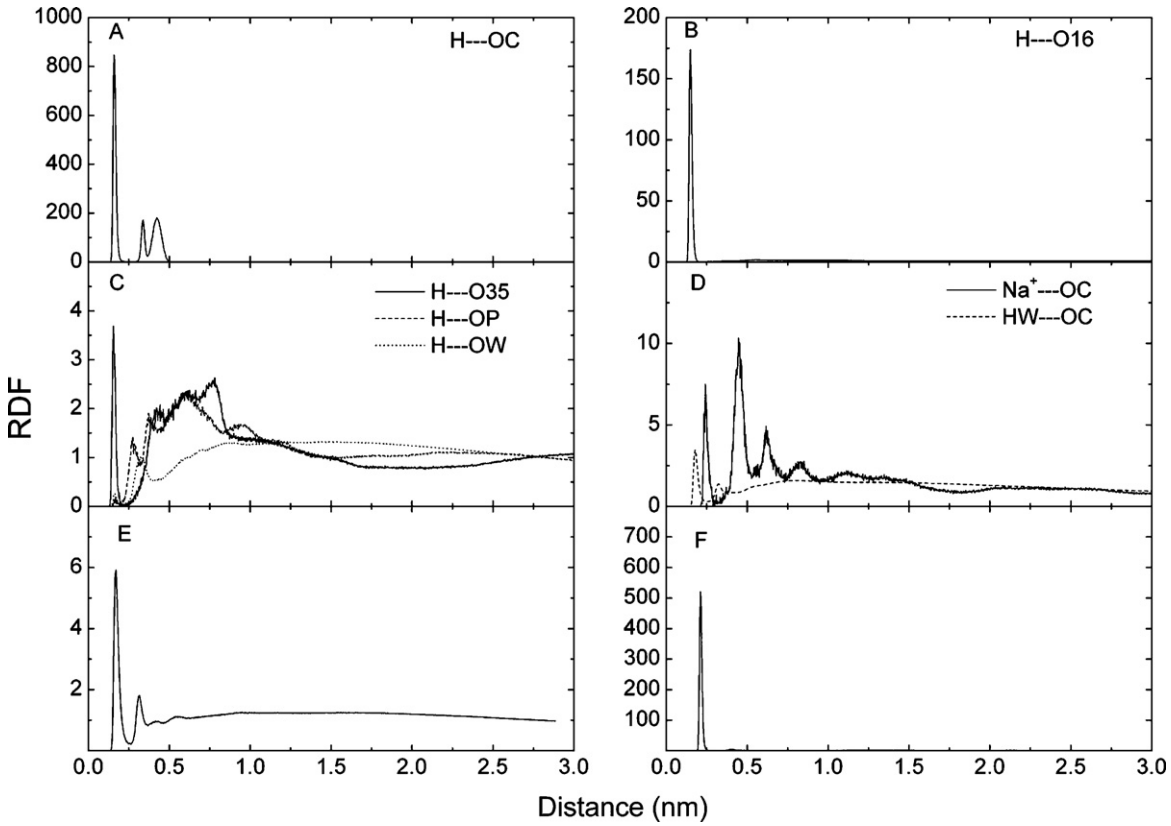

Fig. 5. (A–D) The radial distribution functions (RDFs) for SAL carboxylic (OC), lipid (O16, O35 and OP) and water (OW) oxygen atoms around the hydrogen atom of the hydroxyl group of SAL (H). The RDFs of Na^+ and hydrogen atoms of water (HW) relative to the carboxylic oxygen atoms of SALs are also shown. These RDFs are averaged over the last 20 ns. (E and F) The RDF for water hydrogen atoms around the PCP oxygen atoms (E). The RDF of Na^+ relative to the PCP oxygen atoms is also shown (F). These RDFs are averaged over the last 15 ns.

SAL–POPC system. Since no cluster was found by analyzing the center of mass of SALs, the intermolecular hydrogen bond is formed within single SAL molecules (Fig. 5A). This finding also facilitates to explain the decrease in the number of contacts between SALs and water as shown in Fig. 3. Moreover, oxygen O16 of the oleoyl chain seems more suitable to accept hydrogen atom of SAL than other POPC oxygen atoms including oxygen O35 of palmitoyl chain and those of phosphate group (OP) (Fig. 5B and C). A recent study also observed that cholesterol hydroxyl hydrogen atom preferred to form a hydrogen bond with O16 of POPC bilayer [44]. Finally, hydrogen bonded to water in the interfacial region is not so notable (Fig. 5C and D), which in turn supports the conclusion that SALs were buried into the lipid as discussed above.

The anionic PCPs are most likely to act as hydrogen acceptor, keeping them staying in the lipid–water interface by forming H-bonds with water (Fig. 5E). The RDFs of Na^+ relative to oxygen atoms of SAL carboxylic group (Fig. 5D) and hydroxyl group of PCPs (Fig. 5F) are consistent with the electron density profile (Fig. 4), confirming the coordination of Na^+ with SALs and PCPs in the lipid bilayer. The feature that coordination power of Na^+ with PCP is greater than SAL provides an evidence for the ion-pair formation of uncouplers [6].

The plots of H-bond number among SAL/PCP, POPC bilayer and water are shown in Fig. 6. Snapshots of the distribution of PCP and SAL in POPC bilayer are shown in Fig. 7. The trends are consistent with the RDFs. About four SALs establish H-bond with O16 and two SAL forms intermolecular H-bond. The remainder one SAL has chance to establish H-bond with O35 and water. This could imply that H-bonded to lipid is stronger than to water. The average number of H-bond formed between six PCPs and water is 10, which is nearly equal the most possible number 12 irrespective of the occasion where Na^+ binds to one PCP.

As described in Section 2, N_{Hdon}, N_{Hacc}, E_{HOMO} and E_{LUMO} were also used to represent H-bond capacity. It has been known that highly toxic compounds are associated with low E_{LUMO} values and more H-bond donors [11,19]. However, the prerequisite of bioactivity is the affinity to the target. Previous MD simulation has shown that neutral PCPs H-bonded to the carbonyl oxygen atoms in the POPC bilayer [25]. From present MD simulation, it is

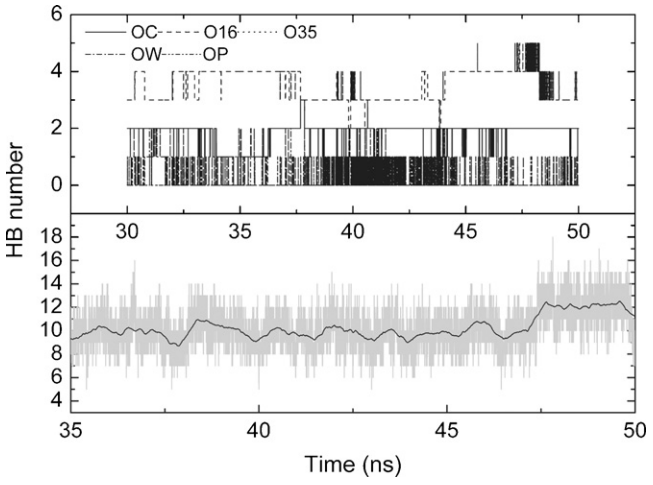

Fig. 6. Top: number of H-bonds among SALs, POPC bilayer and water; bottom: number of H-bonds between PCPs and POPC bilayer. The black curve represents 500 ps running average.

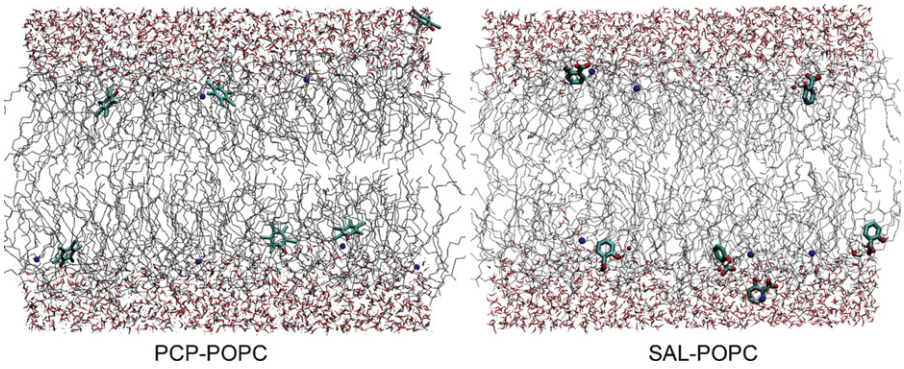

Fig. 7. Snapshots of the distribution of PCP and SAL in the POPC bilayer taken at 50 ns. PCP/SAL is shown as Licorice representation. Lipids are drawn as gray lines with O16 shown as red spheres in SAL–POPC system. Na^+ is drawn as blue spheres and water is drawn as red and white sticks.

reasonable to conclude that un-ionized PCPs, acting as uncouplers, are more toxic to membrane than ionized PCPs. Furthermore, the dissociated SALs, acting as polar narcotics, also display strong affinity to the carbonyl oxygen atom (O16) of the POPC bilayer. Therefore, MD simulations provide a proof for the assumption that polar narcotics are likely to residue in the membrane and exert toxic potency.

4. Conclusions

In this work, the role of hydrophobic and hydrogen bonding molecular descriptors in classifying polar narcotics and uncouplers were investigated by means of SVM. As a consequence, their predictive capabilities were confirmed.

MD simulations were performed to study the equilibrium behaviors of dissociated SAL and PCP molecules in the POPC bilayer as described by area per lipid, electron density, the RDFs and H-bond number. Results were compared with previous MD simulations and differences were discussed. We find that ionic PCPs penetrate less deeply than neutral species in the POPC bilayer due to the formation of H-bonds with water in the region of water–lipid interface. The favorable occupation of PCPs in turn decreases the area per lipid although the effect is not so noticeable. The RDFs and H-bond number profiles further unveil the colorful feature of hydrogen bonding molecular descriptors. The type of H-bond established between SALs and lipid indicates the possible side effects of polar narcotics on membrane. The H-bonds established between either undissociated or dissociated PCPs and the POPC bilayer provide important implications for the uncoupling activity. The distribution of PCPs in the POPC bilayer is accord with the experimental $\log K_{\mathrm{lipw}}$ or calculated $\log K_{\mathrm{ow}}$ values.

One advantage of MD simulations is that the interaction between different components can be studied at atomic level, which may be useful for validating QSARs. For example, the target site of polar narcotics was assumed to be the negatively charged phosphatidyl choline head groups in the membrane by early QSAR studies [19,48]. However, previous and present MD simulations of SALs in different lipid bilayers indicate that it is the carbonyl oxygen atoms (O16) that SALs complex with. The combination of SVM and MD simulations provides a new strategy for elucidating the mechanism of toxic action underlying the corresponding molecular descriptors.

Acknowledgements

The authors gratefully acknowledge financial support for this work from the National Natural Science Foundation (No. 10572033), the Subsidized by the Special Funds for Major State Basic Research Project (No. 2009CB918501) and High Science and Technology Project (No. 2006AA01A124) of China.

Appendix A. Supplementary data

Supplementary data associated with this article can be found, in the online version, at doi:10.1016/j.jmgm.2008.12.007.

References

[1] R.P. Schwarzenbach, B.I. Escher, K. Fenner, T.B. Hofstetter, C.A. Johnson, U. von Gunten, B. Wehrli, The challenge of micropollutants in quatic systems, Science 313 (2006) 1072–1077.
[2] B. Bukowska, S. Kowalska, The presence and toxicity of phenol derivatives—their effect on human erythrocytes, Curr. Top. Biophys. 27 (2003) 43–51.
[3] B.I. Escher, R.P. Schwarzenbach, Partitioning of substituted phenols in liposome–water, biomembrane–water, and octanol–water systems, Environ. Sci. Technol. 30 (1996) 260–270.
[4] B.I. Escher, R.P. Schwarzenbach, Mechanistic studies on baseline toxicity and uncoupling of organic compounds as a basis for modeling effective membrane concentrations in aquatic organisms, Aquat. Sci. 64 (2002) 20–35.
[5] M.W. Toussaint, T.R. Shedd, W.H. van der Schalie, G.R. Leather, A comparison of standard acute toxicity tests with rapid-screening toxicity tests, Environ. Toxicol. Chem. 14 (1995) 907–915.
[6] H. Terada, Uncouplers of oxidative phosphorylation, Environ. Health Perspect. 87 (1990) 213–218.
[7] A.O. Aptula, T.I. Netzeva, I.V. Valkova, M.T.D. Cronin, T.W. Schultz, R. Kühne, G. Schüürmann, Multivariate discrimination between modes of toxic action of phenols, Quant. Struct. Act. Relat. 21 (2002) 12–22.
[8] M.T.D. Cronin, A.O. Aptula, J.C. Duffy, T.I. Netzeva, P.H. Rowe, I.V. Valkova, T.W. Schultz, Comparative assessment of methods to develop QSARs for the prediction of the toxicity of phenols to *Tetrahymena pyriformis*, Chemosphere 49 (2002) 1201–1221.
[9] S. Ren, H. Kim, Comparative assessment of multiresponse regression methods for predicting the mechanisms of toxic action of phenols, J. Chem. Inf. Comput. Sci. 43 (2003) 2106–2110.
[10] S. Ren, Ecotoxicity prediction using mechanism- and non-mechanism-based QSARs: a preliminary study, Chemosphere 53 (2003) 1053–1065.
[11] G. Schüürmann, A.O. Aptula, R. Kuehne, R.U. Ebert, Stepwise discrimination between four modes of toxic action of phenols in the *Tetrahymena pyriformis* assay, Chem. Res. Toxicol. 16 (2003) 974–987.
[12] S. Spycher, E. Pellegrini, J. Gasteiger, Use of structure descriptors to discriminate between modes of toxic action of phenols, J. Chem. Inf. Model. 45 (2005) 200–208.
[13] I. Kahn, S. Sild, U. Maran, Modeling the toxicity of chemicals to *Tetrahymena pyriformis* using heuristic multilinear regression and heuristic back-propagation neural networks, J. Chem. Inf. Model. 47 (2007) 2271–2279.
[14] M. Nendza, M. Müller, Discriminating toxicant classes by mode of action. 2. Physico-chemical descriptors, Quant. Struct. Act. Relat. 19 (2000) 581–598.
[15] M.T.D. Cronin, T.W. Schultz, Pitfalls in QSAR, J. Mol. Struct. (THEOCHEM) 622 (2003) 39–51.
[16] G.M. Maggiora, On outliers and activity cliffss-why QSAR often disappoints, J. Chem. Inf. Model. 46 (2006) 1535.
[17] S.R. Johnson, The trouble with QSAR (or how I learned to stop worrying and embrace fallacy), J. Chem. Inf. Model. 48 (2008) 25–26.
[18] S. Ren, Determining the mechanisms of toxic action of phenols to *Tetrahymena pyriformis*, Environ. Toxicol. 17 (2002) 119–127.
[19] E.U. Ramos, W.H.J. Vaes, H.J.M. Verhaar, J.L.M. Hermens, Quantitative structure–activity relationships for the aquatic toxicity of polar and nonpolar narcotic pollutants, J. Chem. Inf. Comput. Sci. 38 (1998) 845–852.
[20] S. Ren, Classifying class I and class II compounds by hydrophobicity and hydrogen bonding descriptors, Environ. Toxicol. 17 (2002) 415–423.

[21] E. Papa, F. Villa, P. Gramatica, Statistically validated QSARs, based on theoretical descriptors, for modeling aquatic toxicity of organic chemicals in *Pimephales promelas* (*Fathead Minnow*), J. Chem. Inf. Model. 45 (2005) 1256–1266.
[22] J.C. Dearden, M.T.D. Cronin, Y.H. Zhao, O.A. Raevsky, QSAR studies of compounds acting by polar and non-polar narcosis: an examination of the role of polarisability and hydrogen bonding, Quant. Struct. Act. Relat. 19 (2000) 3–9.
[23] T.W. Schultz, M.T.D. Cronin, J.D. Walker, A.O. Aptula, Quantitative structure-activity relationships (QSARs) in toxicology: a historical perspective, J. Mol. Struct. (THEOCHEM) 622 (2003) 1–22.
[24] D. Bemporad, J.W. Essex, Permeation of small molecules through a lipid bilayer: a computer simulation study, J. Phys. Chem. B 108 (2004) 4875–4884.
[25] P. Mukhopadhyay, H.J. Vogel, D.P. Tieleman, Distribution of pentachlorophenol in phospholipid bilayers: a molecular dynamics study, Biophys. J. 86 (2004) 337–345.
[26] Y. Song, V. Guallar, N.A. Baker, Molecular dynamics simulations of salicylate effects on the micro- and mesoscopic properties of a dipalmitoylphosphatidylcholine bilayer, Biochemistry 44 (2005) 13425–13438.
[27] D. Plewczynski, S. Spieser, U. Koch, Assessing different classification methods for virtual screening, J. Chem. Inf. Model. 46 (2006) 1098–1106.
[28] V. Vapnik, Statistical Learning Theory, Wiley, New York, 1998.
[29] Chang, C.C., Lin, C.J., 2001. LIBSVM: a library for support vector machines. Software available at http://www.csie.ntu.edu.tw/~cjlin/libsvm.
[30] M.J. Frisch, G.W. Trucks, H.B. Schlegel, G.E. Scuseria, M.A. Robb, J.R. Cheeseman, V.G. Zakrzewski, J.A. Montgomery Jr., R.E. Stratmann, J.C. Burant, S. Dapprich, J.M. Millam, A.D. Daniels, K.N. Kudin, M.C. Strain, O. Farkas, J. Tomasi, V. Barone, M. Cossi, R. Cammi, B. Mennucci, C. Pomelli, C. Adamo, S. Clifford, J. Ochterski, G.A. Petersson, P.Y. Ayala, Q. Cui, K. Morokuma, D.K. Malick, A.D. Rabuck, K. Raghavachari, J.B. Foresman, J. Cioslowski, J.V. Ortiz, B.B. Stefanov, G. Liu, A. Liashenko, P. Piskorz, I. Komaromi, R. Gomperts, R.L. Martin, D.J. Fox, T. Keith, M.A. Al-Laham, C.Y. Peng, A. Nanayakkara, C. Gonzalez, M. Challacombe, P.M.W. Gill, B. Johnson, W. Chen, M.W. Wong, C. Gonzalez, J.A. Pople, Gaussian 03, Revision C.02, Gaussian Inc., Wallingford, CT, 2004.
[31] C.I. Bayly, P. Cieplak, W.D. Cornell, P.A. Kollman, A well-behaved electrostatic potential based method using charge restraints for deriving atomic charges: the RESP model, J. Phys. Chem. 97 (1993) 10269–10280.
[32] A.W. Schüttelkopf, D.M.F. van Aalten, PRODRG: a tool for high throughput crystallography of protein–ligand complexes, Acta Cryst. D 60 (2004) 1355–1363.
[33] J.F. Nagle, R. Zhang, S. Tristram-Nagle, W. Sun, H.I. Petrache, R.M. Suter, X-ray structure determination of fully hydrated Lα phase dipalmitoylphosphatidylcholine bilayers, Biophys. J. 70 (1996) 1419–1431.
[34] O. Berger, O. Edholm, F. Jähnig, Molecular dynamics simulations of a fluid bilayer of dipalmitoylphosphatidylcholine at full hydration, constant pressure, and constant temperature, Biophys. J. 72 (1997) 2002–2013.
[35] M. Patra, E. Salonen, E. Terama, I. Vattulainen, R. Faller, B.W. Lee, J. Holopainen, M. Karttunen, Under the influence of alcohol: the effect of ethanol and methanol on lipid bilayers, Biophys. J. 90 (2006) 1121–1135.
[36] C. Anézo, A.H. de Vries, H.D. Höltje, D.P. Tieleman, S.J. Marrink, Methodological issues in lipid bilayer simulations, J. Phys. Chem. B 107 (2003) 9424–9433.
[37] B. Hess, H. Bekker, H.J.C. Berendsen, J.G.E.M. Fraaije, LINCS: a linear constraint solver for molecular simulations, J. Comp. Chem. 18 (1997) 1463–1472.
[38] H.J.C. Berendsen, J.P.M. Postma, W.F. van Gunsteren, A. Dinola, J.R. Haak, Molecular dynamics with coupling to an external bath, J. Chem. Phys. 81 (1984) 3684–3690.
[39] T.D. Darden, D. York, L. Pedersen, Particle mesh Ewald: an N log(N) method for Ewald sums in large systems, J. Chem. Phys. 98 (1993) 10089–10092.
[40] M. Patra, M. Karttunen, M.T. Hyvönen, E. Falck, P. Lindqvist, I. Vattulainen, Molecular dynamics simulations of lipid bilayers: major artifacts due to truncating electrostatic interactions, Biophys. J. 84 (2003) 3636–3645.
[41] E. Lindahl, B. Hess, D. van der Spoel, GROMACS 3.0: a package for molecular simulation and trajectory analysis, J. Mol. Model. 7 (2001) 306–317.
[42] Y. Xue, H. Li, C.Y. Ung, C.W. Yap, Y.Z. Chen, Classification of a diverse set of *Tetrahymena pyriformis* toxicity chemical compounds from molecular descriptors by statistical learning methods, Chem. Res. Toxicol. 19 (2006) 1030–1039.
[43] M.A. Villarreal, S.B. Díaz, E.A. Disalvo, G.G. Montich, Molecular dynamics simulation study of the interaction of trehalose with lipid membranes, Langmuir 20 (2004) 7844–7851.
[44] J. Aittoniemi, P.S. Niemelä, M.T. Hyvönen, M. Karttunen, I. Vattulainen, Insight into the putative specific interactions between cholesterol, sphingomyelin, and palmitoyl-pleoyl phosphatidylcholine, Biophys. J. 92 (2007) 1125–1137.
[45] D.E. Elmore, Molecular dynamics simulation of a phosphatidylglycerol membrane, FEBS Lett. 58 (2006) 144–148.
[46] B.I. Escher, R.W. Hunziker, R.P. Schwarzenbach, Interaction of phenolic uncouplers in binary mixtures: concentration-additive and synergistic effects, Environ. Sci. Technol. 35 (2001) 3905–3914.
[47] B.I. Escher, M. Snozzi, R.P. Schwarzenbach, Uptake, speciation, and uncoupling activity of substituted phenols in energy transducing membranes, Environ. Sci. Technol. 30 (1996) 3071–3079.
[48] D.W. Roberts, J.F. Costello, Mechanisms of action for general and polar narcotics: a difference in dimension, QSAR Comb. Sci. 22 (2003) 226–233.